Noise-proofing the repressilator: synchronous long-term oscillations in a synthetic gene circuit

Laurent Potvin-Trottier[†‡] Nathan D. Lord[†] Glenn Vinnicombe[§] Johan Paulsson[†]

Synthetically engineered genetic circuits can perform a wide range of tasks but generally with lower accuracy than natural systems. Here we revisited the first synthetic genetic oscillator, the repressilator[1], and modified it based on principles from stochastic chemistry in single cells. Specifically, we sought to reduce error propagation and information losses, not by adding control loops, but by simply removing existing features. This created highly regular and robust oscillations. Some streamlined circuits kept 14 generation periods over a range of growth conditions and kept phase for hundreds of generations in single cells, allowing cells in flasks and colonies to oscillate synchronously without any coupling between them. Our results show that even the simplest synthetic genetic networks can achieve a precision that rivals natural systems, and emphasize the importance of noise analyses for circuit design in synthetic biology.

Many biological systems show remarkably precise and robust dynamics. For example, the circadian clock in cyanobacteria uses a combination of transcriptional and post-translational control mechanisms[2,3] to keep phase for weeks without entrainment, while displaying robustness to changes in temperature and growth rate[3–5]. Synthetic circuits built from well-characterized parts can also exhibit a wide range of dynamical features – including arithmetic computations[6,7], oscillations[1,8–13], logic gates[14] and edge detection[15] – but often with lower accuracy. For example, the repressilator[1], a now iconic device that helped jump-start the field of synthetic biology 15 years ago, showed clear signs of oscillations using a simple design where three genes inhibit each other's production in a single loop (A⊣B⊣C⊣A). However, only about 40% of cells were found to support oscillations, and those oscillations were quite irregular. Subsequent synthetic oscillators evaluated different control topologies or repression mechanisms[8–13], but most were again quite irregular in both phase and amplitude despite being mathematically designed to display sustained oscillations in a broad range of parameters.

The challenge when designing synthetic circuits to operate reliably in single cells is that biochemical noise can do more than just create different rate constants in different cells. On one hand, simple intrinsic noise can in principle enhance control[16] and even create high-quality oscillations in systems that could not display limit cycles for any rate constants in the absence of noise[17,18]. On the other hand, any component present in low numbers can in principle randomize behavior of the whole system, and a single stochastic signaling step can introduce fundamental constraints[19] that cannot be overcome by any control system. This suggests that simplicity could even help achieve accurate oscillations as long as stochastic effects are accounted for in the design, and that minimal control topologies may be not only be elegant and interesting but also very effective. We therefore revisited the original repressilator to reduce error propagation from the reporter system, from core cellular processes, and from within the circuit itself.

The repressilator consists of three genes – *tetR* from the Tn10 transposon, *cI* from bacteriophage λ and *lacI* from the lactose operon – and each repressor has a C-terminal *ssrA* tag[20] that targets it for degradation (Fig. 1A). The whole circuit was encoded on a low-copy pSC101 plasmid in an *Escherichia coli* strain lacking *lacI*, and a second high-copy ColE1 reporter plasmid encoded GFP under the control of TetR with a modified degradation tag[1,21]. We first reevaluated this circuit using a microfluidic device in which cells are trapped in short channels and newborn cells are washed away by fresh medium[22,23] (Fig. 1A). Tracking reporter levels under the microscope for hundreds of consecutive generations across hundreds of single-cell traces (Methods) revealed clear oscillatory dynamics in all cells (Figs. 1B and S1A), particularly in the *rate* of production (Fig. S1A). This shows that the simple design was sound and that some of the erratic behavior originally reported was due to the limited imaging platforms available at the time.

We next evaluated how much of the noise reflected error propagation from the reporter system. Mathematical predictions have suggested that high-copy ColE1 cloning vectors fluctuate substantially and slowly, due to poorly controlled self-replication, and therefore effectively transmit fluctuations to encoded proteins[24]. Moving the YFP reporter onto the low-copy repressilator plasmid indeed reduced the relative standard deviation in amplitude greatly, from 78% to 36% (Fig. 1D, S2F and S3B). Degradation tagged reporter proteins have also been predicted to potentially have 'retroactivity' effects on oscillations[25] due to competition for shared proteases. Protease competition has in fact been cleverly exploited for improved control in synthetic circuits[13], but stochastic theory[24,26] suggests that saturated degradation enzymes also can create effects related to dynamic instability of microtubules, with large random fluctuations in single cells. Comparing a range of constructs indeed showed that the synthetic degradation tag caused fluctuations to propagate from the reporter proteins to the repressors via the proteolysis system. Surprisingly, however, the 'competing' reporter proteins *accelerated* the degradation of ssrA-tagged substrates (SI §3.1.1). Removing this interference created very regular oscillations, with periods increasing from ~2.4 to ~5.7 generations (Fig. 1D-E, S1B, S2B and S3C). Characterizing the phase drift – the statistical tendency of oscillations in individual cells to go out of phase with each other – showed that on average this circuit oscillates for ~5.5 periods before accumulating half a period of drift (SI §2.5.5).

In cell-free extracts, i.e., without the low-copy noise of single cells, the repressilator has been shown to display the sinusoidal curves expected for harmonic oscillators[27]. However, analyzing the highly asymmetric shape of the time traces in single cells shows that it effectively operates as a *relaxation* oscillator[28], i.e., with a characteristic build-up phase sharply followed by an almost pure dilution and degradation phase until concentrations reach very low levels (Fig. 1D and Box 1). The mathematical conditions for sustained harmonic oscillations – cooperative repression and similar mRNA and protein half-lives[1] – are then

[†]Dept. of Systems Biology, Harvard Medical School, 200 Longwood Ave, Boston, MA 02115, USA [‡] Biophysics Program, Harvard University, Cambridge, MA [§] Dept. of Engineering, University of Cambridge, Cambridge CB2 1PZ, UK

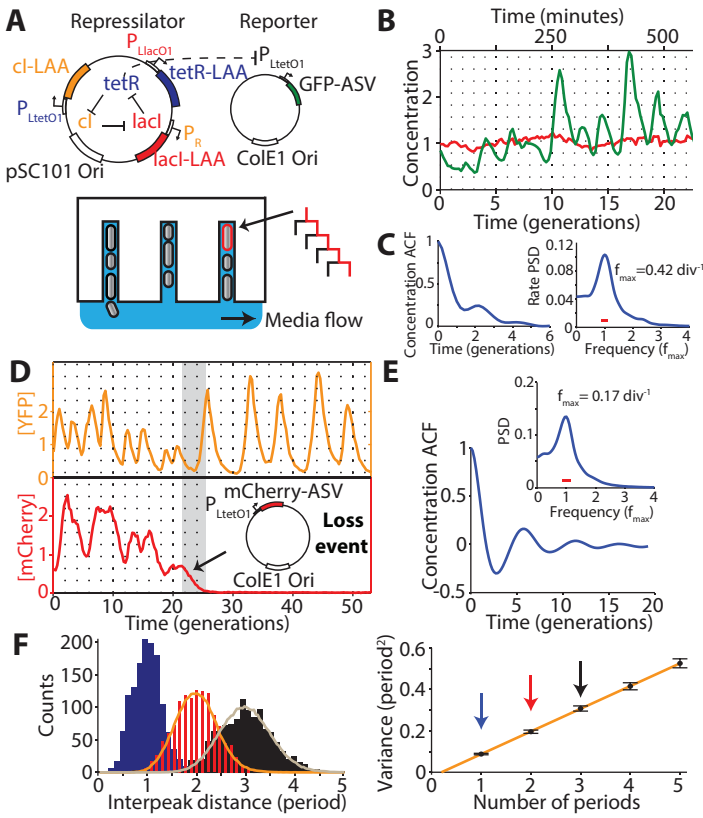

Figure 1: Reducing reporter interference. A) Schematics of the original repressilator plasmids as described in text and microfluidic device where *E. coli* cells are diffusively fed in growth channels and daughters eventually are washed away. B) Typical time trace of a single cell for original repressilator (NDL332). The GFP concentration (green trace) oscillates noisily while a constantly expressed RFP (red trace) stays constant. Both traces were normalized to their means. C) Autocorrelation functions (ACF) and power spectral densities (PSD) were calculated over the whole population (2,706 generations) and demonstrate oscillations with a mean period of 2.4 average division time. D) Top: oscillations are more regular when the reporter is expressed on the repressilator plasmid rather than on a separate high-copy plasmid (Fig. S3). Some cells irreversible shift period from ~2.5 to ~5.5 generations. Bottom: The period change was invariably connected to a loss of the separate mCherry-ASV-expressing reporter plasmid. Analysis of e.g. empty plasmid vectors, various reporter proteins and reporter degradation tags (Fig. S7), and circuits with and without repressor degradation (SI §3.1 and 3.3) show that the interference was caused by the reporter *ssrA* degradation tag where the last three amino acids were substituted to ASV. E) ACF and PSD for the YFP expressing repressilator without separate reporter plasmid (LPT25), calculated over all 8,694 total cell divisions observed. Average period was 5.6 generations. Reporter protein close to fluorescence detection limit at troughs, and the actively degraded repressors should be much lower yet. The PSD was normalized by peak frequency, with width of the window function indicated by red line. F) Histograms of interpeak distances for one, two and three periods in blue, red and black respectively. Orange and grey lines were obtained by summing two or three samples (respectively) from the blue distribution. Consecutive periods are thus independent. Panel on right shows that the variance in period grows linearly with the number of periods elapsed (LPT25).

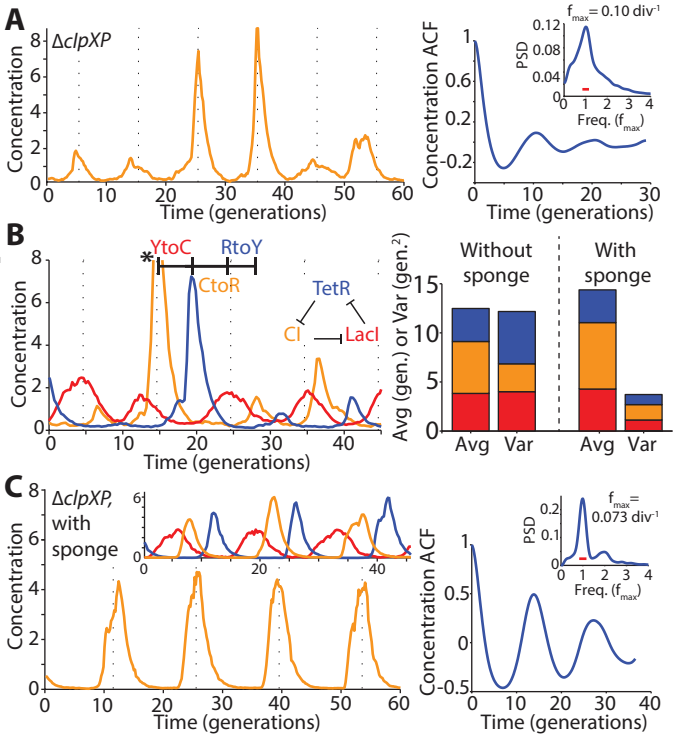

Figure 2: Identifying and eliminating inherent sources of error. A) Typical time trace in Δ*clpXP* cells (LPT61) where repressors are not degraded. ACF and PSD calculated over 5,356 cell divisions. The average period was 10 generations, and the correlation coefficient was 0.1. Dashed vertical lines are separated by an average period to illustrate periodicity in A-C. B) (Left) Time trace of multi-reporter repressilator (Δ*clpXP*, LPT113). TetR represses the production of YFP (yellow trace), LacI inhibits the production of CFP (blue trace) and CI represses the production of RFP (red trace). Peak indicated by asterisk not shown due to its high amplitude of 11.5 units. (Right) Interpeak distances evaluated for YFP to CFP (YtoC, red), CFP to RFP (CtoR, yellow) and RFP to YFP (RtoY, blue) without (LPT113, n = 163, 150 and 173) and with the titration sponge (plasmid with P_{Ltet} binding sites, LPT117 and LPT127, combined, n = 109, 86 and 116). Respective contributions to the average and variance shown by bar plot. The RtoY part of the oscillation (induction of YFP, low TetR levels) represents 27% of the period, but contributes 44% of the variance. Addition of the P_{Ltet} titration sponge brings down the variance almost fourfold. C) Example time trace of single reporter repressilator with P_{Ltet}-mCherry-ASV (Δ*clpXP*, LPT64), along with ACF and PSD calculated over 3,695 generations. Oscillations have an average period of 14 generations and a correlation coefficient of 0.5 after one period. Inset shows a time trace from the triple reporter repressilator without degradation and with titration sponge (LPT127, color scheme as in B).

less relevant, but it becomes key to reduce the heterogeneity in the build-up and dilution phase (Box 1, SI §4.3.1) since stochastic effects otherwise fundamentally compromise the system's ability to keep track of time. Specifically, if the production phase for each of the repressors involves a low number of stochastic production events, statistical variation in that number will cause heterogeneity in peak amplitude, which then to some extent creates heterogeneity in the subsequent dilution and decay period. If peak protein abundances are low, random degradation events or uneven partitioning of molecules at cell division will in turn cause heterogeneity in the decay and dilution process. In fact, increasing peak abundances should only help marginally unless the repression thresholds are also increased appropriately (Box 1), since the last few steps contribute disproportionally to the variance (Box 1, SI §4.2.2).

Motivated by these results, we eliminated repressor degradation by removing the *ssrA* degradation tags from the repressors, by using a Δ*clpXP* strain, or both (SI §3.3). These circuits indeed oscillated in all cells, with a period of ~10 generations.

Box 1 | Relaxation oscillations of the repressilator

Depending on parameters, simple repressilators can produce traditional harmonic oscillations with sinusoidal trajectories, as observed *in vitro*, or relaxation oscillations with separate build-up and relaxation phases (panels below) as we observe experimentally in single cells (middle panel). Due to low abundance fluctuation effects, single cells can in principle also achieve stable oscillations without the traditional requirements of cooperative repression and feedback delays (simulation example in left panel, details in SI). However, having low abundances introduces other constraints. For example, using Poisson communications theory[29] we demonstrate (SI §A) hard limits on the ability of such systems to keep track of time, in terms of the average number of molecules N at the peak of the oscillations, even if a repression control system could remember time series of decay events. For circuits like the actual repressilator, where repression is set by the current repressor level, the constraints are more severe yet, and limited both by heterogeneity in N and the inherent noise of the first-order elimination process until levels reach the repression threshold S. Variation in N can be reduced if repressors approach a steady state where production is balanced by elimination (left panel). Noise in N also only has a damped effect on the time to reach a threshold because that time approximately depends *logarithmically* on N/S: doubling N only adds one more half-life before reaching S. However, substantial noise can arise towards the end of each decay phase if the repression threshold S is too low, as the last few steps then dominate the total decay time (right panel and inset). Specifically, the average length of the decay phase is $\sum_{i=S}^{N} 1/i \approx \log(N/S)$ while the variance is $\sum_{i=S}^{N} 1/i^2 \approx 1/S$ in units of protein half-lives (for details see SI §4.2.2), creating an optimal threshold S_{opt} that minimizes the CV in the decay time. Increasing N should only significantly reduce this CV if $S > S_{opt}$, have virtually no effect if $S < S_{opt}$, and decrease the CV in proportion to $\sqrt{N}$ if S is close to S_{opt} (Fig. S10E). Finally, the exponential nature of the decay phase allows the repressilator to be robust to growth conditions: changes in N/S are logarithmically damped in their effects on the average period. Though N and S change with conditions, for many repressors they may change with similar factors that cancel out in the ratio, e.g. because conditions with less gene expression (lowering N) also tend to produce smaller cell volumes (lowering S).

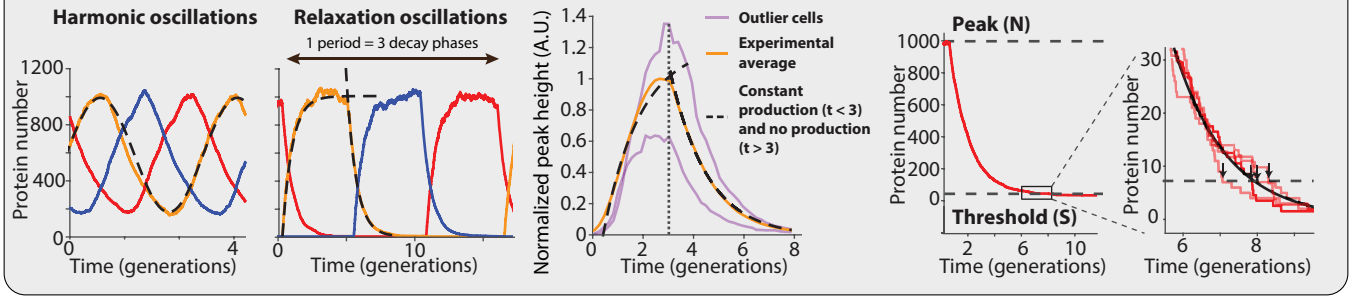

However, as predicted the noise in the period was only slightly reduced (Figs. 2A and S2C). To pinpoint the reason we built a circuit with compatible fluorescent reporter proteins for each repressor. Analyzing the variance in the three interpeak distances showed that the noisiest phase was when TetR levels were low (Fig. 2B). We then estimated the protein abundances from the partitioning errors at cell division (SI §3.5), and found that the derepression of the TetR controlled promoter occurs at an extremely low threshold. The theory suggests that the regularity could be greatly improved if this threshold was raised, e.g. using a 'sponge' of repressor binding sites that soaks up small numbers of TetR molecules. The high-copy reporter plasmid included in the original repressilator design in fact already carried binding sites for TetR, and simply reintroducing it greatly reduced noise in all steps (Fig. 2B) whereas similar sponges for CI and LacI had minor effects (Fig. S5D) as expected. Titration may in fact be a particularly useful way to increase the thresholds because it can also help create sharp switches[30] (SI §4.3), which may or may not be necessary for oscillations in single cells but generally should increase accuracy.

These changes created a streamlined repressilator with highly regular oscillations that peak every ~14 generations (Fig. 2C). Each repressor spends several generations at virtually undetectable concentrations (SI §3.5) followed by several generations at concentrations that completely saturate repression. The amplitude still displays some variation (Fig. S9D), but because the time it takes to dilute levels from a peak amplitude of N to a threshold of S depends logarithmically on N/S, little variation in amplitude is transmitted to the timing (Box 1, Fig. S9E). Indeed the phase drift was only ~14% per period (Fig. S2D), i.e., on average the circuit should oscillate for ~18 periods before accumulating half a period of drift (SI §2.5.5). The theory shows that similar accuracy should be possible in systems where dilution in growing cells is replaced by first order degradation, and that it is not the slowness itself that creates accuracy, but the absolute number of proteins at peaks and troughs.

The periods of circadian clocks, as measured in hours, are often robust to changes in growth conditions. However, other intracellular oscillators may need periods that instead are robust relative to internal physiological time scales such as the generation times. Synthetic circuits generally do not display either type of quantitative robustness because periods depend on so many different parameters that change with conditions. That is in principle also true for the circuits above: as conditions change, plasmid copy numbers, RNA degradation, gene expression, cell volume, etc. change in non-trivial ways. However, the logarithmic dampening that makes individual periods insensitive to fluctuations in peak amplitudes (Box 1) is also predicted to make the number of generations per period insensitive to growth conditions (Box 1). Indeed we found that the circuit retained the 14 generation period under all conditions tested (Fig. 3A), including growth at 25-37°C and in conditioned medium from early stationary phase culture where cells become much smaller and almost spherical. The combination of robustness to conditions and great inherent precision suggest that cells could display macroscopic, population-scale oscillations without cell-cell communication. We therefore synchronized a liquid culture and maintained it in early exponential phase (Methods). We indeed found that whole flasks oscillated autonomously, with a period of the expected ~14 generations (Fig. 3B, S Movie 1). We also imaged the growth of large colonies originating from single cells containing the triple reporter repressilator. Because only the cells at the edges of the

colonies grow significantly, cells in the interior were arrested in different repressilator phases, creating ring-like expression profiles much like the seasonal growth rings seen in tree stumps (Fig. 3C and S5A). The regularity originated in the autonomous behavior of single cells – no connections were introduced and cells kept their own phase when merging into areas where the neighboring cells had a different phase (Fig. S5C).

The results above illustrate the importance of understanding genetic networks at the level of stochastic chemistry, particularly for synthetic circuits where the noise has not been shaped by natural selection and where the heterologous components and reporters used may interfere with cells. We hypothesize that if statistical properties are systematically measured and the mechanisms are iteratively redesigned based on general stochastic principles, the next generation of synthetic circuits could rival or even surpass the precision of natural systems.

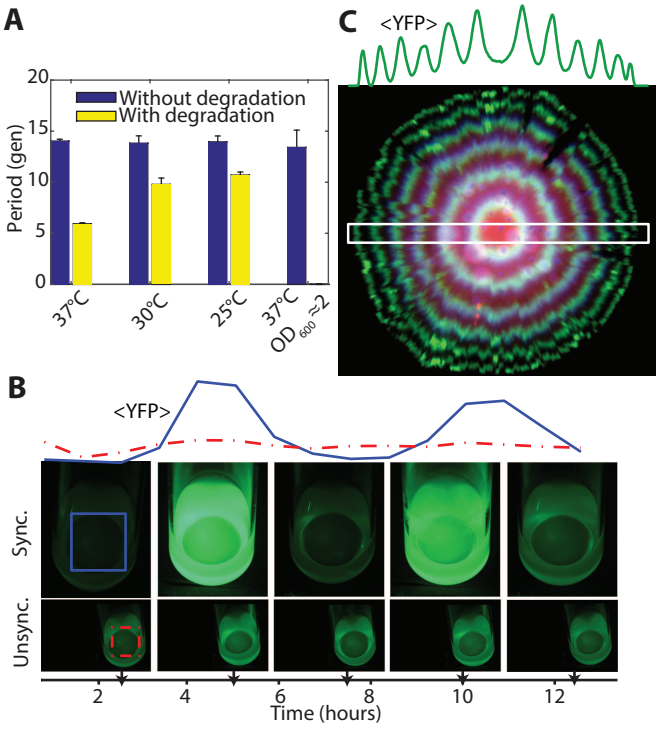

Figure 3: The modified repressilator shows great robustness to growth conditions. A) The repressilator without degradation and with titration sponge (LPT64) has a period of 14 generations at different temperatures (blue bars, division time of 27, 40 and 59 min for 37°C, 30°C and 25°C respectively) and in conditioned media (OD_{600} ~2, doubling time of 44 min). Repressilator with repressor degradation (LPT25) shows a varying period (yellow bars, doubling time of 26, 34 and 52 min for 37°C, 30°C and 25°C respectively). Error bars indicate STD on the first maximum of the ACF obtained by bootstrapping. B) Cells containing multi-reporter repressilator without repressor degradation and with P_{Ltet}-peptide-ASV plasmid ($\Delta clpXP$, LPT117) were grown in liquid culture in 25mL flasks. After the culture was initially synchronized with IPTG, it was kept in exponential phase via dilution. Average YFP intensity shown for colored square area, with unsychronized culture for comparison. C) A ~5 mm diameter colony of cells with the triple reporter colony (LPT117) reveals tree-like ring patterns in FP levels. The average YFP intensity is reported for the slice in the white rectangle. The decrease in RFP levels towards the edge of the colony is likely due to different response to stationary phase of its promoter.

[1] M. B. Elowitz & S. Leibler, "A synthetic oscillatory network of transcriptional regulators," *Nature*, 403, 335–338, 2000.

[2] M. Nakajima, K. Imai, H. Ito, T. Nishiwaki, Y. Murayama, H. Iwasaki, T. Oyama, & T. Kondo, "Reconstitution of Circadian Oscillation of Cyanobacterial KaiC Phosphorylation in Vitro," *Science*, 308, 414–415, 2005.

[3] S.-W. Teng, S. Mukherji, J. R. Moffitt, S. de Buyl, & E. K. O'Shea, "Robust circadian oscillations in growing cyanobacteria require transcriptional feedback.," *Science*, 340, 737–40, May 2013.

[4] I. Mihalcescu, W. Hsing, & S. Leibler, "Resilient circadian oscillator revealed in individual cyanobacteria," *Nature*, 430, 81–85, 2004.

[5] J. R. Chabot, J. M. Pedraza, P. Luitel, & A. van Oudenaarden, "Stochastic gene expression out-of-steady-state in the cyanobacterial circadian clock," *Nature*, 450, 1249–1252, 2007.

[6] A. E. Friedland, T. K. Lu, X. Wang, D. Shi, G. Church, & J. J. Collins, "Synthetic gene networks that count.," *Science*, 324, 1199–202, May 2009.

[7] R. Daniel, J. R. Rubens, R. Sarpeshkar, & T. K. Lu, "Synthetic analog computation in living cells," *Nature*, 2013.

[8] E. Fung, W. W. Wong, J. K. Suen, T. Bulter, S. G. Lee, & J. C. Liao, "A synthetic gene-metabolic oscillator," *Nature*, 435, 118–122, 2005.

[9] J. Stricker, S. Cookson, M. R. Bennett, W. H. Mather, L. S. Tsimring, & J. Hasty, "A fast, robust and tunable synthetic gene oscillator," *Nature*, 456, 516–519, 2008.

[10] M. Tigges, T. T. Marquez-Lago, J. Stelling, & M. Fussenegger, "A tunable synthetic mammalian oscillator," *Nature*, 457, 309–312, 2009.

[11] T. Danino, O. Mondragón-Palomino, L. Tsimring, & J. Hasty, "A synchronized quorum of genetic clocks.," *Nature*, 463, 326–30, Jan. 2010.

[12] O. Mondragón-Palomino, T. Danino, J. Selimkhanov, L. Tsimring, & J. Hasty, "Entrainment of a population of synthetic genetic oscillators.," *Science*, 333, 1315–9, Sept. 2011.

[13] A. Prindle, J. Selimkhanov, H. Li, I. Razinkov, L. S. Tsimring, & J. Hasty, "Rapid and tunable post-translational coupling of genetic circuits," *Nature*, Apr. 2014.

[14] J. Bonnet, P. Yin, M. E. Ortiz, P. Subsoontorn, & D. Endy, "Amplifying Genetic Logic Gates," *Science*, 2013.

[15] J. J. Tabor, H. M. Salis, Z. B. Simpson, A. a. Chevalier, A. Levskaya, E. M. Marcotte, C. a. Voigt, & A. D. Ellington, "A synthetic genetic edge detection program.," *Cell*, 137, 1272–81, June 2009.

[16] J. Paulsson, O. G. Berg, & M. Ehrenberg, "Stochastic focusing: fluctuation-enhanced sensitivity of intracellular regulation," *Proc Natl Acad Sci USA*, 97, 7148–7153, 2000.

[17] J. M. G. Vilar, H. Y. Kueh, N. Barkai, & S. Leibler, "Mechanisms of noise-resistance in genetic oscillators.," *Proc Natl Acad Sci USA*, 99, 5988–92, Apr. 2002.

[18] a. J. McKane & T. J. Newman, "Predator-Prey Cycles from Resonant Amplification of Demographic Stochasticity," *Physical Review Letters*, 94, p. 218102, June 2005.

[19] I. Lestas, G. Vinnicombe, & J. Paulsson, "Fundamental limits on the suppression of molecular fluctuations," *Nature*, 467, 174–178, 2010.

[20] K. Keiler, P. Waller, & R. Sauer, "Role of a peptide tagging system in degradation of proteins synthesized from damaged messenger RNA," *Science*, 271, 990–993, 1996.

[21] J. B. Andersen, C. Sternberg, L. K. Poulsen, S. P. Bjorn, M. Givskov, & S. Molin, "New unstable variants of green fluorescent protein for studies of transient gene expression in bacteria," *Appl Environ Microbiol*, 64, 2240–2246, 1998.

[22] P. Wang, L. Robert, J. Pelletier, W. L. Dang, F. Taddei, A. Wright, & S. Jun, "Robust growth of Escherichia coli," *Curr Biol*, 20, 1099–1103, 2010.

[23] T. M. Norman, N. D. Lord, J. Paulsson, & R. Losick, "Memory and modularity in cell-fate decision making.," *Nature*, 503, 481–6, Nov. 2013.

[24] J. Paulsson & M. Ehrenberg, "Noise in a minimal regulatory network: plasmid copy number control," *Q Rev Biophys*, 34, 1–59, 2001.

[25] T. Moriya, M. Yamamura, & D. Kiga, "Effects of downstream genes on synthetic genetic circuits," *BMC Systems Biology*, 8, p. S4, 2014.

[26] O. G. Berg, J. Paulsson, & M. Ehrenberg, "Fluctuations and quality of control in biological cells: zero-order ultrasensitivity reinvestigated," *Biophysical journal*, 79, 1228–1236, 2000.

[27] H. Niederholtmeyer, Z. Sun, Y. Hori, E. Yeung, A. Verpoorte, R. M. Murray, & S. J. Maerkl, "Rapid cell-free forward engineering of novel genetic ring oscillators," *eLife*, p. e09771, 2015.

[28] B. van der Pol, "On relaxation-oscillations," *Philosophical Magazine*, 2, 978–992, 1926.

[29] S. Verdú, "Poisson communication theory," *Invited talk, March*, 25, 1999.

[30] R. Brewster, F. Weinert, H. Garcia, D. Song, M. Rydenfelt, & R. Phillips, "The Transcription Factor Titration Effect Dictates Level of Gene Expression," *Cell*, 156, 1312–1323, Mar. 2014.

Supplementary Information is available in the online version.

Acknowledgements We thank M. Elowitz for the repressilator plasmids, D. Landgraf for strains and plasmids, P. Cluzel for the fluorescent proteins, SG Megason and his lab for their microscope, R. Chait and M. Baym for the macroscope and C. Saenz for technical help on the microfluidics device. Some work was performed at the Harvard Medical School Microfluidics Facility and the Center for Nanoscale Systems, a member of the National Nanotechnology Infrastructure Network supported by NSF award ECS-0335765. LPT acknowledges fellowship support from the Natural Sciences and Engineering Research Council of Canada (NSERC) and the Fonds de recherche du Québec – Nature et technologies. This work was supported by NIH Grant GM095784 and NSF Award 1137676.

Author contribution L.P.T. and J.P. conceived the study and did the theoretical analysis with G.V. Experiments and data analysis were done by L.P.T. with help from N.D.L. All authors wrote the paper.

Author information Reprints and permissions information is available at www.nature.com/reprints. The authors declare no competing financial interests. Readers are welcome to comment on the online version of the paper. Correspondence and requests for materials should be addressed to J.P. (johan_paulsson@harvard.edu)

METHODS SUMMARY

Strain construction All strains were built from *Escherichia coli* MC4100 strain using standard molecular biology techniques. The strains and plasmids used are listed in the Supplementary information along with more detailed description of their construction.

Microfluidic device fabrication Fabrication of the wafer was carried out using standard UV photolithography in a clean room environment. The protocol is described in details in the Supplementary information. Dimethyl siloxane monomer (Sylgard 184) was mixed in a 10:1 ratio with curing agent, defoamed, poured onto the silicon wafer, degassed for 1 hour and cured at 65°C for 1 hour. Individual chips were then cut and the inlets and outlets were punched with a biopsy puncher. Bonding to KOH-cleaned cover slips was ensured using oxygen plasma treatment (30 sec at 50 W and O_2 pressure at 170 mTorr) on the day the experiments start. The chips were then incubated at 95°C for at least 30 min to reinforce the bonding.

Cell preparation and device loading *E. coli* strains were grown overnight in LB with appropriate antibiotics and diluted 1:100 ~2-3 hours before the beginning of the experiments in imaging media, consisting of M9 salts, 10% (v/v) LB, 0.2% (w/v) glucose, 2 mM $MgSO_4$, 0.1 mM $CaCl_2$, 1.5 μM thiamine hydrochloride and 0.85 g/L Pluronic F-108 (Sigma Aldrich, included as a passivating agent). The cells were loaded into the device at OD_{600} 0.2-0.4, and centrifuged on a custom-machined holder that could fit into a standard table-top centrifuge at 5000 g for 10 min to insert them into the side-channels. The feeding channels were connected to syringes filled with imaging media using Tygon tubing (VWR), and media was pumped using syringe pumps (New Era Pump System) initially at a high rate of 100 μL/min for 1 hour, to clear the inlets and outlets. The media was then pumped at 5-10 μL/min for the duration of the experiment and cells were allowed to adapt to the device for multiple hours before imaging was started.

Microscopy and image acquisition Images were acquired using a Nikon Ti inverted microscope equipped with a temperature-controlled incubator, an Orca R2 CCD camera (Hamamatsu), a 60X Plan Apo oil objective (NA 1.4, Nikon), an automated xy-stage (Ludl) and light engine LED excitation source (Lumencor). All experiments were performed at 37°C. Microscope control was done with MATLAB (Mathworks) scripts interfacing with μManager[31]. Typical exposure was low (50-100 msec) in order to reduce photobleaching, and the reporter channels were acquired using 2x2 binning (CCD chip dimension of 1344 x 1024 pixels, effective pixel size of 129nm x 129nm). 16 bits TIFF images were taken every 5-8 minutes, and focal drift was controlled via the Nikon PerfectFocus system, as well as a custom routine based on z-stack images of a sacrificial position. The following filter sets were used for acquisition: GFP (Semrock GFP-3035B), RFP (Semrock mCherry-A), YFP (Semrock YFP-2427A) and CFP (Semrock CFP-2432A).

Autocorrelation function and power spectrum estimation The autocorrelation functions were estimated by averaging the correlation functions of the individual cells, as it was more robust to outliers, and using the unbiased estimator. Similar functions were obtained by taking directly the autocorrelation of the population, but needed manual curation of the data to remove dead cells or filaments.

$$A(\tau) = \left\langle \frac{\langle (x_i(t) - \langle x_i(t)\rangle_t)(x_i(t+\tau) - \langle x_i(t)\rangle_t)\rangle_t}{\langle x_i(t)^2\rangle_t} \right\rangle_i \quad (1)$$

where $x_i(t)$ is the production rate or the concentration (indicated in the figure caption) of the i^{th} cell at time t. Averaging of the correlations functions of the cells was done taking into account the finite length of the time series (each cell has a different number of samples for a specific time lag). If A_i is the autocorrelation of cell i,

$$\hat{A}[j] = \frac{\sum_i (L_i - j)\hat{A}_i[j]}{\sum_i (L_i - j)} \quad (2)$$

with $A(j\Delta t) = \hat{A}[j]$, Δt the time between images, j the discrete delay index and L_i the number of points in time trace i. The brackets are used to emphasize discrete sampling. The autocorrelations were cropped to a constantly decreasing envelope to keep only time lags with good estimates. This resulted in correlation functions very similar to the ones obtained by using the biased estimator, albeit with a slightly larger envelope.

The power spectrum was then estimated by taking the discrete Fourier transform (DFT) of the windowed autocorrelation function[32,33]:

$$P[k] = \mathrm{DFT}_N(a[m]) \quad (3)$$

where DFT_N is the N point DFT and $a[m]$ is the windowed symmetric autocorrelation:

$$a[m] = \begin{cases} \hat{A}\left[|M-m|\right] w[m] & \text{for } 0 \le m \le 2M \\ 0 & \text{for } 2M < m \le N \end{cases} \quad (4)$$

and $w[m]$ is a window function. Then,

$$P[k] = P(\omega)|_{\omega = 2\pi k/N} \quad (5)$$

$$P(\omega) = \frac{1}{2\pi}\int_{-\pi}^{\pi} X(\theta) W(\omega - \theta) d\theta \quad (6)$$

where $X(\omega)$ is the power spectrum of the signal and $W(\omega)$ the Fourier transform of the window function. We are therefore sampling the power spectrum of the signal convolved with $W(\omega)$. This is a consistent estimator of the power spectrum (it converges to the actual power spectrum as the amount of data goes to infinity)[34]. We used a triangular window function to avoid negative spectral leakage, and the length of the window function ($2M$) was chosen to maximize the resolution without introducing too much noise (50-225 frames, depending on the period of the oscillations). The approximate resolution loss was indicated by a red line of width $2\pi/M$ ($1/(M\Delta t)$) in the figures.

Period histograms and phase drift estimation Peak-to-peak distances were evaluated by finding maxima using the *findpeaks* MATLAB function. The traces were first smoothed using a 3 or 5 points moving average and peaks were rejected if they were closer than 3 or 5 frames to avoid double counting, or smaller than the average of the trace. The peaks were then manually curated; this was especially useful for the noisy oscillators. Note that the average period was slighly shorter than the first maximum of the autocorrelation, most likely because longer periods have higher intensities and thus more weights in the correlation (but not in the period histrogram).

The period histograms were made by using the peak-to-peak distance. The squared error on the n^{th} period grew linearly with n, as expected for this type of oscillator undergoing a random walk in phase. We therefore used the coefficient of variation (CV, standard deviation divided by the mean) of the period as an indicator of phase drift; the normalization makes comparison between oscillators of different frequencies straightforward.

Most of the strains had a phase drift of 30-35% per period; except for the repressilator without degradation but with the titration sponge, where it was only 14%. Since the variance increases linearly, we can express the variance for n periods (σ_n^2) as a function of the variance for one (σ_1^2):

$$\begin{aligned} \sigma_n^2 &= n\sigma_1^2 \\ \sigma_n &= \sigma_1\sqrt{n} \\ &= \langle \text{period} \rangle \times \text{CV}\sqrt{n} \end{aligned}$$

Hence, it would take ~13 periods (~179 generations) to obtain a standard deviation of half a period.

Another measure of the phase drift is the *average* time to reach half a period of phase drift, or the average first passage time. This could be calculated by drawing randomly directly from the period histogram until the first time the phase drift is reached, because subsequent periods were exceptionally well approximated as independent (Fig. 4A). This creates a distribution of first passage time, and after 10^5 iterations, we converge on an average first passage time of ~ 18 periods (~ 240 generations), again for the repressilator without degradation with titration (LPT64).

[31] A. Edelstein, N. Amodaj, K. Hoover, R. Vale, & N. Stuurman, "Computer control of microscopes using microManager.," *Current protocols in molecular biology*, Chapter 14, p. Unit14.20, Oct. 2010.

[32] R. B. Blackman & J. W. Tukey, *The measurement of power spectra.* New York, NY: Dover Publications, 1958.

[33] A. V. Oppenheim & R. W. Schafer, *Discrete-time signal processing*. Upper Saddle River, NJ: Prentice Hall, 3 ed., 1989.

[34] G. M. Jenkins & D. G. Watts, *Spectral Analysis.* 1968.